Title

Kv1.3 inhibition as a potential microglia-targeted therapy for Alzheimer's disease: preclinical proof of concept

Journal

Brain, 141(2)

ISSN

0006-8950

Authors

Maezawa, Izumi

Nguyen, Hai M

Di Lucente, Jacopo

et al.

Publication Date

2018-02-01

DOI

10.1093/brain/awx346

Peer reviewed

doi:10.1093/brain/awx346 BRAIN 2018: 141; 596–612 | 596

BRAIN
A JOURNAL OF NEUROLOGY

$K_v1.3$ inhibition as a potential microglia-targeted therapy for Alzheimer's disease: preclinical proof of concept

Izumi Maezawa,[1,*] Hai M. Nguyen,[2] Jacopo Di Lucente,[1] David Paul Jenkins,[2] Vikrant Singh,[2] Silvia Hilt,[3] Kyoungmi Kim,[4] Srikant Rangaraju,[5] Allan I. Levey,[5] Heike Wulff[2,*] and Lee-Way Jin[1,6,*]

*These authors contributed equally to this work.

Microglia significantly contribute to the pathophysiology of Alzheimer's disease but an effective microglia-targeted therapeutic approach is not yet available clinically. The potassium channels $K_v1.3$ and $K_{ir}2.1$ play important roles in regulating immune cell functions and have been implicated by *in vitro* studies in the 'M1-like pro-inflammatory' or 'M2-like anti-inflammatory' state of microglia, respectively. We here found that amyloid-β oligomer-induced expression of $K_v1.3$ and $K_{ir}2.1$ in cultured primary microglia. Likewise, *ex vivo* microglia acutely isolated from the Alzheimer's model 5xFAD mice co-expressed $K_v1.3$ and $K_{ir}2.1$ as well as markers traditionally associated with M1 and M2 activation suggesting that amyloid-β oligomer induces a microglial activation state that is more complex than previously thought. Using the orally available, brain penetrant small molecule $K_v1.3$ blocker PAP-1 as a tool, we showed that pro-inflammatory and neurotoxic microglial responses induced by amyloid-β oligomer required $K_v1.3$ activity *in vitro* and in hippocampal slices. Since we further observed that $K_v1.3$ was highly expressed in microglia of transgenic Alzheimer's mouse models and human Alzheimer's disease brains, we hypothesized that pharmacological $K_v1.3$ inhibition could mitigate the pathology induced by amyloid-β aggregates. Indeed, treating APP/PS1 transgenic mice with a 5-month oral regimen of PAP-1, starting at 9 months of age, when the animals already manifest cognitive deficits and amyloid pathology, reduced neuroinflammation, decreased cerebral amyloid load, enhanced hippocampal neuronal plasticity, and improved behavioural deficits. The observed decrease in cerebral amyloid deposition was consistent with the *in vitro* finding that PAP-1 enhanced amyloid-β uptake by microglia. Collectively, these results provide proof-of-concept data to advance $K_v1.3$ blockers to Alzheimer's disease clinical trials.

1 Department of Pathology and Laboratory Medicine, University of California Davis Medical Center, 2805 50th Street, Sacramento, CA 95817, USA
2 Department of Pharmacology, University of California Davis, 451 Health Sciences Drive, Davis, CA 95616, USA
3 Department of Biochemistry and Molecular Medicine, University of California Davis, 2700 Stockton Blvd, Sacramento, CA 95817, USA
4 Department of Public Health Sciences, University of California Davis, One Shields Avenue, Med Sci 1-C, Davis, CA 95616, USA
5 Department of Neurology and Alzheimer's Disease Research Center, Emory University, 201 Dowman Drive, Atlanta, GA 30322, USA
6 Alzheimer's Disease Center, University of California Davis Medical Center, 4860 Y Street, Suite 3900, Sacramento, CA 95817, USA

Correspondence to: Izumi Maezawa
Department of Pathology and Laboratory Medicine, University of California Davis Medical Center,
2805 50th Street, Sacramento, CA 95817, USA
E-mail: imaezawa@ucdavis.edu

Received July 14, 2017. Revised October 9, 2017. Accepted October 30, 2017. Advance Access publication December 18, 2017

Correspondence may also be addressed to:
Lee-Way Jin
Department of Pathology and Laboratory Medicine, University of California Davis Medical Center,
2805 50th Street, Sacramento, CA 95817, USA
E-mail: lwjin@ucdavis.edu

Heike Wulff
Department of Pharmacology, University of California Davis, 451 Health Sciences Drive, Davis, CA 95616, USA
E-mail: hwulff@ucdavis.edu

Keywords: potassium channel; microglia; Alzheimer's disease; neuroinflammation; amyloid-β

Abbreviations: AβO = amyloid-β oligomer; FSB = (*E*,*E*)-1-fluoro-2,5-*bis*(3-hydroxycarbonyl-4-hydroxy)styrylbenzene; LTP = long-term potentiation; LPS = lipopolysaccharide; MAPK = mitogen-activated protein kinase; PAP-1 = 5-(4-phenoxybutoxy)psoralen; TBS = Tris-buffered saline

Introduction

Although several drugs for symptoms of Alzheimer's disease have now been approved, they do not alter disease progression and their benefits are at most modest, indicating an urgent need for new target discovery. Multiple lines of evidence have implicated a significant role of microglia and associated neuroinflammation in Alzheimer's disease. A generally accepted hypothesis states that activated microglia release cytotoxic substances and pro-inflammatory cytokines that cause neuronal damage and aggravate Alzheimer's disease pathology (Heneka *et al.*, 2015). A network-based analysis of whole-genome gene-expression profiling and genotypic data obtained from 1647 Alzheimer's disease and non-demented brain samples highlighted the immune/microglia module as the molecular system most strongly associated with the pathophysiology of Alzheimer's disease (Zhang *et al.*, 2013). An even stronger correlation was recently found between a similar immune/microglial module and Alzheimer's disease with large-scale protein co-expression network analysis (Seyfried *et al.*, 2017). Immune receptor genes expressed in microglia or myeloid cells, such as *TREM2* and *CD33*, are among the few genes that impose moderate risk for the development of Alzheimer's disease (Karch *et al.*, 2014). Despite this progress, a microglia-targeting therapeutic agent has not been available clinically. Results from several clinical trials using generic anti-inflammatory agents have been disappointing, mainly due to inadequate brain penetration of existing non-steroid anti-inflammatory drugs, suboptimal doses, unknown molecular targets, and non-specific activities (Rogers, 2008). A large-scale prevention trial with naproxen and celecoxib was stopped early because of drug safety concerns. These setbacks, however, should prompt investigations to develop novel anti-inflammatory agents with known specific targets, better brain penetrance, and low toxicities.

The voltage-gated potassium channel $K_v1.3$ plays an important role in immune cell activation by modulating Ca^{2+} signalling (Wulff *et al.*, 2007; Feske *et al.*, 2015). Through K^+ efflux, $K_v1.3$ helps maintain a negative membrane potential, which provides the driving force for Ca^{2+} entry through the store-operated inward-rectifier calcium channels like the Ca^{2+} release activated Ca^{2+} channel ORAI, or transient receptor potential cation channels. Accordingly, $K_v1.3$ blockers have been demonstrated to inhibit microglia-mediated neurotoxicity in culture (Fordyce *et al.*, 2005) and to protect mice from microglia-mediated radiation-induced brain injury *in vivo* (Peng *et al.*, 2014). Interestingly, blockade of $K_v1.3$ appears to specifically inhibit certain signal pathways but not others in the molecular cascade leading to microglia activation (Fordyce *et al.*, 2005). A systems pharmacology-based study identified functional roles for $K_v1.3$ in pro-inflammatory microglial activation (Rangaraju *et al.*, 2017) while electrophysiological studies by our group demonstrated upregulated $K_v1.3$ expression in microglia acutely isolated from the infarct areas of mice subjected to experimental stroke (Chen *et al.*, 2016). *In vitro* studies with primary microglia further demonstrated association of high $K_v1.3$ expression with the lipopolysaccharide (LPS)-induced 'M1-like' activation and inflammatory cytokine production (Nguyen *et al.*, 2017). Interestingly, in 'alternatively activated M2-like' microglia, such as those activated by interleukin 4 (IL-4), $K_v1.3$ expression was silenced and instead the inward-rectifier $K_{ir}2.1$, another K^+ channel often expressed in myeloid cells and involved in regulating their function (Kettenmann *et al.*, 2011; Feske *et al.*, 2015), was highly upregulated (Nguyen *et al.*, 2017). $K_v1.3$ inhibition, therefore, could be used to fine-tune the pattern/state of microglia activation as an anti-inflammatory approach. $K_v1.3$ expression has also been described in some neurons. However, in neurons $K_v1.3$ is typically part of heteromultimers with $K_v1.1$, $K_v1.2$ and $K_v1.6$ subunits (Helms *et al.*, 1997) and has a different pharmacology distinct from the $K_v1.3$ homotetramers found in T cells, microglia and macrophages (Chandy *et al.*, 2004; Wulff *et al.*, 2009). Therefore, a relatively selective pharmacological targeting of $K_v1.3$ in microglia is feasible. We have developed a highly specific $K_v1.3$ blocker PAP-1 [5-(4-phenoxybutoxy)psoralen; Schmitz *et al.*, 2005] and demonstrated that this small molecule effectively prevents autoimmune diabetes in a rat model and treats psoriasis in a humanized xenograft model in mice (Beeton *et al.*, 2006; Kundu-Raychaudhuri *et al.*, 2014).

Moreover, we have shown that the expression of $K_v1.3$ is elevated in human Alzheimer's disease brains and the elevation is limited to microglia, suggesting that $K_v1.3$ is a pathologically relevant microglial target in Alzheimer's disease (Rangaraju *et al.*, 2015). Here we examined the effects of $K_v1.3$ blockade in cellular and mouse models of Alzheimer's disease, using the brain penetrant PAP-1 as a pharmacological tool.

Materials and methods

Study approval

All protocols involving mouse models were approved by the Institutional Animal Care and Use Committee of the University of California Davis. Human brain samples were drawn from the brain repositories of University of California Davis Alzheimer's Disease Center and Emory University Alzheimer's Disease Research Center. The collection and use of brain samples were approved by the respective Institutional Review Board.

Mice

C57BL/6 and APP/PS1 [B6.Cg-Tg(APPswe,PSEN1dE9)85Dbo/Mmjax] mice were originally purchased from the Jackson laboratory. The line Tg6799 5xFAD mice was obtained from Dr Robert Vassar at Northwestern University.

Tissue cultures and acute isolation of microglia

Primary microglia were prepared from mixed glia cultures established from newborn mice with the 'shaking-off' method as described (Maezawa *et al.*, 2011). Hippocampal slice cultures were prepared from 7-day-old C57BL/6 mice as described (Maezawa *et al.*, 2011) and cultured for 10 days *in vitro* before use.

Microglia were acutely isolated from adult brains without culturing as described (Jin *et al.*, 2015). Briefly, brains were dissociated enzymatically with a Neural Tissue Dissociation Kit (Miltenyi Biotec). Microglia were subsequently purified by the magnetic-activated cell sorting using anti-CD11b magnetic beads (Miltenyi Biotec).

Electrophysiology on cultured and acutely isolated microglia

Whole-cell patch-clamp experiments on cultured or acutely isolated microglia were performed as previously described (Chen *et al.*, 2016; Nguyen *et al.*, 2017). For details, see Supplementary material.

Production and administration of amyloid-β oligomer

Amyloid-β oligomer (AβO) was prepared following a standard procedure (Lambert *et al.*, 1998) except that the amyloid-$\beta_{1\text{-}42}$ peptide (Bachem) was diluted with Opti-MEM® culture medium instead of the F12 medium originally described, before incubation at 4°C for 24 h to generate oligomers. Our preparation has been extensively characterized (Maezawa *et al.*, 2006, 2008). To ensure consistency of quality, a random sample from each batch was imaged using atomic force microscopy to characterize the size and shape of the aggregates, and the biological activities were confirmed by determining AβO's neurotoxic activity and ability to rapidly induce exocytosis of MTT formazan, as described (Maezawa *et al.*, 2006, 2008; Hong *et al.*, 2007). For treatment, primary microglia cells were plated onto 6-well plates (5×10^5 cells/well) or 12-well plates (3×10^5 cells/well) in Dulbecco's modified Eagle medium (DMEM) with 10% foetal bovine serum. After 24 h, culture medium was changed to Opti-MEM® and AβO was freshly diluted and added at indicated concentrations with and without PAP-1. The cultures were incubated for another 24 h before used for quantitative polymerase chain reaction (qPCR) and western blotting.

Quantitative PCR

Total RNA from primary microglia, acutely isolated microglia, and tissue samples were extracted using RNeasy® Plus Mini Kit (Qiagen) or RNeasy® Plus Universal Mini Kit (Qiagen). RNA samples from acutely isolated microglia were further reverse-transcribed and pre-amplified as we previously described (Horiuchi *et al.*, 2017). The result was normalized to β-actin. The primer sequences used are listed in Supplementary Table 1. For β-actin the commercially available primer set Mouse-ACTB (Applied Biosystems) was used. Relative cDNA levels for the target genes were analysed by the 2-ΔΔCt method using *Actb* as the internal control for normalization.

Immunohistochemical staining and quantification

Immunohistochemistry using Vectastain Elite ABC and diaminobenzidine (DAB) on formalin-fixed, paraffin-embedded human brain sections and quantification was performed as previously described (Rangaraju *et al.*, 2015). Briefly, for quantification using ImageJ, the raw images were deconvoluted using the deconvolute plugin into brown (DAB) and haematoxylin channels. Then, the images were thresholded and converted to binary images for quantitative analysis. The $K_v1.3$ immunoreactivity in each image was estimated as the proportion of the image area occupied by Iba1 positive microglia. From the Alzheimer's disease and non-Alzheimer's disease control brains, three adjacent slides were immunostained, and from each section, five random images were obtained for analysis using the same settings.

Immunofluorescence staining and quantification was performed as previously described (Jin *et al.*, 2015). Briefly, microglia cells cultured on cover slip, hippocampal slices and frozen brain sections (20 µm) were fixed in 4% paraformaldehyde and stained with anti-Aβ1-42 (1:200; Millipore), anti-CD68 (1:200; Serotec), anti-CD11b (1:200; AbD Serotec), anti-Iba-1 (1:200, Wako Chemical), anti-$K_v1.3$ (1:200, NeuroMab), or anti-NeuN (1:200, Cell Signaling) overnight at 4°C, followed by respective Alexa Fluor®-conjugated secondary antibodies (1:700; Invitrogen). The amyloid deposits were also detected by 400 nM FSB. Immunostained slides were imaged under a

Nikon Eclipse E600 microscope and photographed by a digital camera (SPOT RTke, SPOT Diagnostics) or under an Olympus FV1000 spectrum confocal microscope. Photomicrographs were randomly taken in a blind fashion from each culture condition or within a defined anatomic region. The images were transformed to 8-bit grayscale and analysed by the ImageJ program. The photography and analysis of immunoreactivity were conducted in an investigator-blinded manner.

Formalin-fixed, paraffin-embedded human tissue sections were immunostained with anti-$K_v1.3$ (1:150; NeuroMab) overnight at 4°C, followed by anti-Iba-1 (1:200; Wako) for 3 h at room temperature, and then Alexa Fluor® 594-conjugated anti-rabbit antibody (1:700) and Alexa Fluor® 488-conjugated anti-mouse antibody (1:700), respectively. Sections were then incubated with 0.1% Sudan black for 10 min to eliminate autofluorescence, followed by 400 nM FSB for 20 min.

Propidium iodide uptake, Fluoro-Jade® C assay, ELISA, NFκB assay, and nitric oxide quantification

The propidium iodide (PI) uptake assay to assess neuronal damage, ELISA quantification of cytokines, nitric oxide (NO) quantification, and NFκB assay were conducted as previously described (Maezawa *et al.*, 2011). For the Fluoro-Jade® C assay, fixed hippocampal slices were placed onto gelatin coated slides and stained with Fluoro-Jade® C (Histo-Chem Inc.) according to the manufacturer's instruction.

Induction of hippocampal long-term potentiation by high frequency stimulation

The preparation of mouse hippocampal slices, and the induction of long-term potentiation (LTP) by high frequency stimulation of the Schaffer collateral afferents were conducted as we previously described (Maezawa, 2017) and are described in detail in the Supplementary material.

Cell/tissue homogenate preparation and western blot analysis

To obtain cell lysates, cells were washed with ice-cold PBS and incubated with a lysis buffer (150 mM NaCl, 10 mM NaH_2PO_4, 1 mM EDTA, 1% Triton™ X-100, 0.5% SDS) with protease inhibitor cocktail and phosphatase inhibitor (Sigma). Equivalent amounts of protein were analysed by 4–15%Tris-HCl gel electrophoresis (Bio-Rad). Proteins were transferred to polyvinylidene difluoride membranes and probed with antibodies. Visualization was enabled using enhanced chemiluminescence (GE Healthcare Pharmacia). The following primary antibodies (dilutions) were used: anti-$K_v1.3$ (1:700, NeuroMab), anti-phosphor-p38MAPK (1:1000, Cell Signaling), anti-p38MAPK (1:1000, Cell Signaling), and anti-GAPDH (1:2000, Cell Signaling). Secondary antibodies were HRP-conjugated anti-rabbit or anti-mouse antibody (1:1000, GE Healthcare).

Brain tissue samples from APP/PS1 treated with PAP-1 or control diet were fractionated into Tris-buffered saline (TBS)-soluble and TBS-insoluble, SDS-soluble fractions to assess the solubility of amyloid-β species. Briefly brain tissues were homogenized in TBS with protease inhibitors, followed by centrifugation (100 000*g*, 30 min, at 4°C). The supernatants were collected as the TBS-soluble fraction. The pellets were homogenized in 2% SDS with protease inhibitors, followed by centrifugation (100 000*g*, 30 min, at 4°C). The supernatants were collected as the TBS-insoluble, SDS-soluble fraction.

Neurobehavioural tests

The neurobehavioural tests, including open field test, novel object recognition test, and step-through passive avoidance test, were conducted in a fashion in which the scorers were blind to the treatment of the mice. The detailed methods are described in the Supplementary material.

Stereotactic intrahippocampal injection

Mice were first anaesthetized using 3% isoflurane and then restrained onto a stereotaxic apparatus. A small incision was made to expose the skull and a 1.0 mm burr hole was drilled. AβO (40 μM in artificial CSF), or vehicle (artificial CSF), was injected using a Hamilton syringe with a 27-gauge needle into the hippocampus by using the following coordinates (mm from bregma): −1.8 anterior/posterior, ±1.7 medial/lateral, and −1.9 dorsal/ventral, at a rate of 0.2 μl/min, 2 μl each side. Before waking, mice received 0.05 mg/kg of buprenorfine subcutaneously and were allowed to recover on an isothermal pad at 36°C.

PAP-1 exposure levels

Total PAP-1 plasma and brain concentrations were determined by LC-MS analysis using a Waters Acquity UPLC (Waters) interfaced to a TSQ Quantum Access Max mass spectrometer (Thermo Fisher Scientific) as described in the Supplementary material.

Statistics

All results were expressed as the mean ± standard error (SE). Normality of the data distribution was determined using the Shapiro-Wilk test. For group comparisons in means, paired or unpaired Student's *t*-test or one- or two-way ANOVA, as appropriate, were conducted using the SigmaStat 3.1 (Systat Inc.). When the overall ANOVA was significant, Bonferroni's multiple comparison procedure was carried out to maintain the family-wise error rate at 0.05. The significance level for the two-sided analyses was set at $P < 0.05$.

Results

Enhanced $K_v1.3$ and $K_{ir}2.1$ expression and activity in AβO-stimulated microglia

We previously showed that AβO, composed of amyloid-$\beta_{1\text{-}42}$ peptide, at low (5–200) nanomolar concentrations is a robust microglia activator (Maezawa *et al.*, 2011). We also

showed that functional polarization of microglia induces a differential K^+ channel expression pattern—while the classic M1-polarizing LPS induces high current densities of $K_v1.3$ and no $K_{ir}2.1$ current, the M2-polarizing IL-4 induces large $K_{ir}2.1$ currents and no $K_v1.3$ current (Nguyen *et al.*, 2017). As these two major microglial K^+ channels regulate Ca^{2+} signalling instrumental for differential activation profiles, we investigated their expression/activity in cultured primary microglia treated with AβO. Similar to LPS, AβO significantly upregulated $K_v1.3$ at both transcript (Fig. 1A) and protein (Fig. 1B and C) levels. Whole-cell voltage-clamp revealed outward rectifying currents induced by AβO, with biophysical properties characteristic of homotetrameric $K_v1.3$ channels typically expressed on immune cells (Fig. 1D), including a half-activation ($V_{1/2}$) value of −28.4 mV in the Boltzmann fit of normalized peak currents (Fig. 1E) and use-dependent inactivation elicited by repetitive depolarization steps (Fig. 1F). Pharmacological characterization showed that the currents were sensitive to the $K_v1.3$ specific blockers ShK-186 (Tarcha *et al.*, 2012), margatoxin (MgTX; Garciacalvo *et al.*, 1993), and PAP-1 (Fig. 1G), with IC_{50} values of 68.5 pM, 79.7 pM, and 6.5 nM, respectively, in good agreement with existing literature. AβO induced a significant increase in $K_v1.3$ current density compared to unstimulated microglia (Fig. 1H), consistent with the increased $K_v1.3$ protein level as shown by western blotting (Fig. 1B) and immunocytochemistry (Fig. 1C). Interestingly, unlike LPS, AβO also induced an increase in Ba^{2+}-sensitive $K_{ir}2.1$ current density (Fig. 1I) that was similar in magnitude to the IL-4-induced $K_{ir}2.1$ current increases (Nguyen *et al.*, 2017), suggesting that AβO induces a microglial activation state that is more complex than previously defined M1- or M2-like polarization. Consistent with this notion, AβO induced microglial expression of IL-1β, TNF-α, and IL-6 traditionally associated with LPS-induced polarization as well as CD86, Arg1, and CD206 traditionally associated with IL-4-induced polarization (Supplementary Fig. 1).

$K_v1.3$ is required for amyloid-β oligomer-induced microglial activation and microglial neurotoxicity

Compared to $K_{ir}2.1$, the pharmacological tools for $K_v1.3$ are far better developed; therefore, we focused our study on the AβO-induced $K_v1.3$ upregulation. We previously showed that AβO induces an activated microglial profile, including proliferation, activation of p38MAPK and NF-κB, NO production, as well as microglia-mediated neurotoxicity (Maezawa *et al.*, 2011). This profile can be induced at concentrations ~200-fold lower than those required for direct neuronal killing, suggesting that early accumulation of AβO in the preclinical stages of Alzheimer's disease could cause significant indirect, microglia-mediated neurotoxicity. To determine if $K_v1.3$ activity is required for AβO-induced microglial activation and associated neurotoxicity, we used the small-molecule $K_v1.3$ inhibitor PAP-1 as a pharmacological probe. In some experiments, the general microglial activation inhibitor doxycycline was used for comparison. PAP-1 blocked AβO-induced microglia proliferation (Fig. 2A) and expressions of pro-inflammatory mediators (Fig. 2D) in a dose-dependent manner. PAP-1 also blocked AβO-induced NF-κB activation (Fig. 2B), NO generation (Fig. 2C), and p38MAPK phosphorylation (Fig. 2E), suggesting that the microglial activating effects of AβO require $K_v1.3$ activity. We further tested $K_v1.3$ inhibition using hippocampal slice cultures, a model allowing microglia and neurons to interact. We previously showed that in this model system, AβO caused substantial microglial activation and associated neurotoxicity mediated by NO, released by activated microglia (Maezawa *et al.*, 2011). Figure 2F shows that AβO treatment of hippocampal slices enhanced CD11b immunoreactivity as well as neurotoxicity, indicated by increased PI uptake and Fluoro-Jade® C labelling, and decreased NeuN labelling (Supplementary Fig. 2). PAP-1 co-incubation substantially mitigated the above changes, similar to doxycycline (Fig. 2F and Supplementary Fig. 2). PAP-1 treatment also significantly reduced the NO level in the hippocampal culture medium [AβO/vehicle: 16.1 ± 0.42 (means ± SE) versus AβO/PAP-1: 6.73 ± 0.50 nM/μg total protein, $n = 3$, $P < 0.001$], consistent with the result obtained from isolated microglia cultures (Fig. 2C).

It was reported that minocycline, a tetracycline inhibitor of microglial activation, and inducible nitric oxide synthase (iNOS) reduction, prevented hippocampal LTP disruption by amyloid-β (Wang *et al.*, 2004), suggesting that microglial activation and NO production contribute to amyloid-β synaptotoxicity. However, the microglial contribution to hippocampal LTP is by no means conclusive in view of the pleotropic, non-microglial effects of minocycline (Griffin *et al.*, 2010). Because PAP-1 selectively targets microglial $K_v1.3$ and inhibits AβO-induced microglial neurotoxicity as well as NO production in hippocampal slices, we tested whether PAP-1 was able to rectify hippocampal LTP deficit using the same induction paradigm as Wang *et al.* (2004). AβO application to the slices blocked hippocampal LTP induction at 20–100 nM, within the range of concentrations that enhanced the expression of microglial $K_v1.3$. Significantly, in the presence of PAP-1, hippocampal LTP induction was not impaired by AβO and was recovered to the control (non-AβO, vehicle-treated) level (Fig. 2G and H). This result is consistent with the notion that AβO at low nanomolar concentrations impairs hippocampal LTP through $K_v1.3$-dependent microglial activation.

Elevated expression of microglial $K_v1.3$ in brains of Alzheimer's transgenic models and Alzheimer's disease patients

To validate the *in vivo* significance of $K_v1.3$ in Alzheimer's disease, we examined brains from the widely used

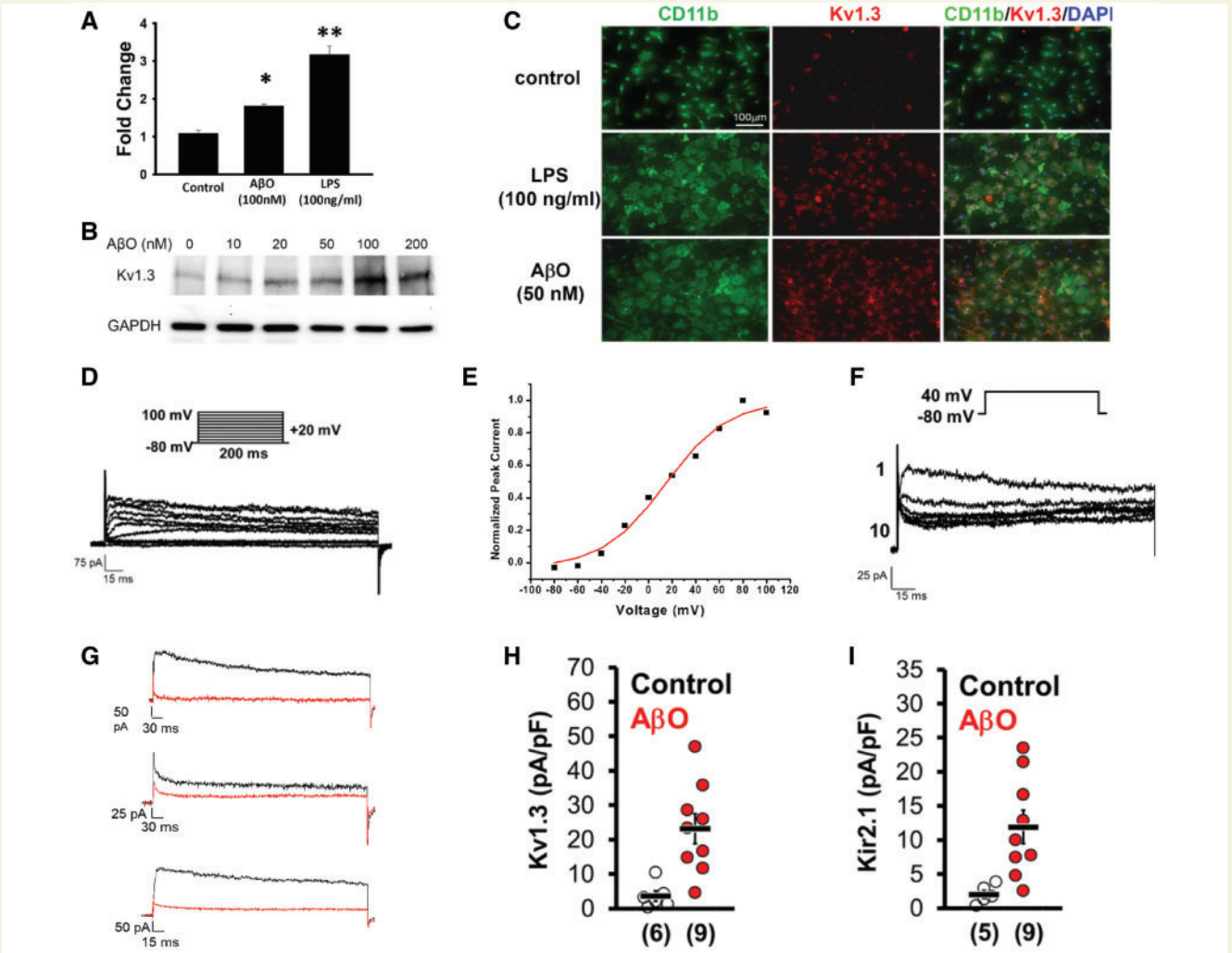

Figure 1 AβO enhanced the expression and activity of $K_v1.3$ in microglia. Cultured primary microglia were treated with AβO or LPS at indicated concentrations for 24 h and used for the following assays. Numerical data are presented by mean ± SE and were analysed by one-way ANOVA with Bonferroni multiple comparisons versus control (vehicle-treated group). (**A**) qPCR showed that both AβO and LPS treatment increased the levels of $K_v1.3$ transcript. $n = 3$, $^*P < 0.05$ and $^{**}P < 0.001$. (**B**) Representative western blotting from four independent experiments showed a dose-dependent increase in $K_v1.3$ protein level following AβO treatment. The cropped blots are presented in the interest of clarity. For quantification, see Supplementary Fig. 8. (**C**) The increase in $K_v1.3$ protein was confirmed by immunocytochemistry, which showed enhanced $K_v1.3$ immunoreactivity in AβO- or LPS- treated microglia. Scale bar = 100 μm. (**D–I**) Electrophysiological characterization of AβO (50 nM)-stimulated cultured microglia. Currents elicited by voltage steps from −80 to 100 mV in 20 mV increments (**D**) with Boltzmann fit of normalized peak currents (**E**) rendering a $V_{1/2} = -28.4$ mV. (**F**) Use-dependent inactivation elicited by repetitive depolarization from −80 to +40 mV (1 pulse/s for 10 pulses). (**G**) Pharmacological characterization: K^+ currents elicited from cultured microglia stimulated with AβO are sensitive to the peptidic $K_v1.3$ blockers ShK-186 and MgTX as well as the small molecule PAP-1. IC_{50}s were determined by testing five concentrations of the respective blockers on three independent cells and fitting the normalize current inhibition to the Hill equation: ShK-186 (68.5 pM), MgTX (79.7 pM), PAP-1 (6.8 nM). (**H**) Current density plot showing $K_v1.3$ channel current expression in control cultured microglia (3.62 ± 1.47 pA/pF; $n = 6$) and AβO treated microglia (23.17 ± 4.34 pA/pF; $n = 9$; $P = 0.0036$). (**I**) Current density plot showing $K_{ir}2.1$ channel current expression in control cultured microglia (2.02 ± 0.64 pA/pF; $n = 5$) and AβO-treated microglia (11.90 ± 2.44 pA/pF; $n = 9$; $P = 0.012$).

Alzheimer's mouse model 5xFAD (Oakley *et al.*, 2006), in which AβO is the major toxic amyloid-β species able to activate microglia to contribute to neuroinflammation (Hong *et al.*, 2009; Xiao *et al.*, 2013; Heneka *et al.*, 2015). Immunofluorescence showed enhanced $K_v1.3$ immunoreactivity in microglia in 5xFAD mice compared to non-transgenic wild-type littermates, especially in areas around amyloid plaques, highlighted by the amyloid dye FSB (Fig. 3A and Supplementary Fig. 3). The $K_v1.3$-positive areas co-localized with areas immunoreactive to CD11b and Iba-1, markers for myeloid cells (Fig. 3A and B), consistent with our previous observations that $K_v1.3$ is typically expressed highest in microglia in the brain (Rangaraju *et al.*, 2015). Similar results were obtained using the other Alzheimer's transgenic model called APP/PS1 (Jankowsky *et al.*, 2004) (Supplementary Fig. 3).

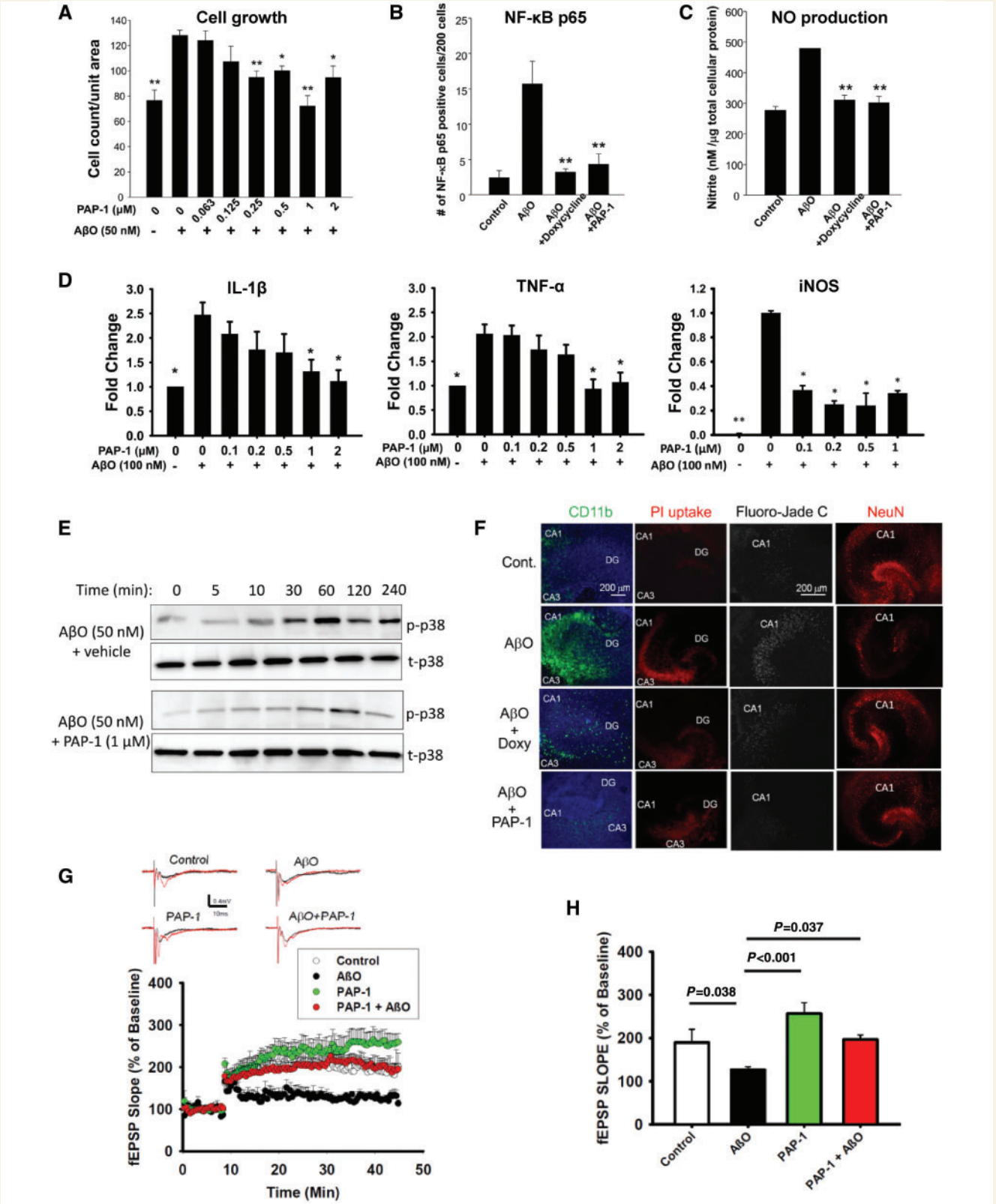

Figure 2 AβO-induced microglial activation and microglial neurotoxicity require $K_v1.3$. (**A–D**) Primary microglia were treated with AβO (50 or 100 nM) and PAP-1 at indicated concentrations. Data were analysed using one-way ANOVA with Bonferroni multiple comparisons versus control (AβO-treated, no PAP-1) group. (**A**) PAP-1 inhibited AβO-induced microglia proliferation in a dose-dependent manner (24 h treatment; $n = 5/6$; $^{*}P < 0.05$ and $^{**}P < 0.001$). (**B**) Microglia after the indicated treatment for 2 h were immunostained for p65 or NFκB to mark cells with NFκB activation. Numbers of p65-immunoreactive cells/200 DAPI-labelled cells were determined. AβO-induced NFκB activation was reduced by PAP-1 (1 μM) or doxycycline (20 μM) treatment ($n = 4$; $^{**}P < 0.001$). (**C**) NO production was measured in the conditioned medium

(continued)

To confirm that the enhanced $K_v1.3$ expression translates to enhanced channel activity, we acutely isolated microglia from adult 5xFAD and wild-type littermate mice and performed voltage-clamp recordings. The procedure to isolate microglia in general took ~1 h, and the cells, without further culturing, were immediately used for recording. While microglia from wild-type littermates showed minimal $K_v1.3$ current density, those from 4, 6, and 10 month-old 5xFAD mice showed significantly increased $K_v1.3$ channel activity (Fig. 3C–E). $K_{ir}2.1$ in microglia of 5xFAD mice also showed sustained high current density at 4, 6, and 10 months of age, reminiscent of the result seen in AβO-treated cultured microglia. The $K_{ir}2.1$ activity was significantly higher in 5xFAD microglia than in wild-type microglia at 4 and 10 months but not at 6 months due to a comparable high activity in wild-type microglia at that age (Fig. 3C, D and F). Interestingly, at 15 months when amyloid plaques were still abundant, the $K_v1.3$ and $K_{ir}2.1$ current densities in 5xFAD microglia were both reduced and no longer significantly different from wild-type microglia (Fig. 3E and F). Quantification of the level of the $K_v1.3$ transcript in acutely isolated microglia also showed age-dependent changes in $K_v1.3$ expression parallel to its channel activity (Supplementary Fig. 4). A similar increase of microglial $K_v1.3$ transcript was also observed in APP/PS1 mice (Fig. 6E).

To verify the *in vivo* significance of microglial $K_v1.3$ in human Alzheimer's disease, our previous immunohistochemical study showed that $K_v1.3$ is almost exclusively expressed in microglia in post-mortem human brains and that $K_v1.3$ expression is substantially increased and associated with amyloid-β plaques in pathologically confirmed Alzheimer's disease cases in the frontal cortex (Rangaraju *et al.*, 2015). We extended this observation to the entorhinal cortical region, where Alzheimer's disease pathologies are robust in the early stage Alzheimer's disease. Again, $K_v1.3$ immunoreactivities were significantly increased in Alzheimer's disease patients (Fig. 4A and B). Combined immunofluorescence using FSB, anti-Iba1, and anti-$K_v1.3$ showed that $K_v1.3$ was localized to a majority of Iba1-immunoreactive microglial cell bodies or processes (Fig. 4C, arrowheads), and its immunoreactivities were accentuated around amyloid-β plaques (Fig. 4A and C). The increase in $K_v1.3$ protein level was in part due to increased $K_v1.3$ transcript level in Alzheimer's disease brains (Fig. 4D).

In vivo effects of $K_v1.3$ blockade by PAP-1 in microglia activation, hippocampal long-term potentiation induction, and memory deficit

Because PAP-1 mitigated the effects of AβO on hippocampal LTP in acutely prepared slices (Fig. 2G and H), we asked if PAP-1 could restore the AβO-induced, hippocampus-dependent memory deficit *in vivo*. To administer PAP-1 to mice, we used oral regimens to mimic treatments in humans, but refrained from oral gavage to avoid undue stress to the animals. PAP-1 dissolved in a mix of the semi-synthetic triglyceride miglyol and condensed milk was quickly consumed by mice and a dose of 100 mg/kg p.o. resulted in high micromolar PAP-1 levels in plasma and several brain regions (Fig. 5A). For example, total hippocampal tissue concentrations peaked at 23 μM at 2 h and exceeded 2 μM for 15 h following ingestion, which, considering PAP-1's IC_{50} of 2 nM for $K_v1.3$ inhibition and its protein binding of 98%, was sufficient to exert a pharmacodynamic effect (Schmitz *et al.*, 2005; Beeton *et al.*, 2006). We found that mice receiving bilateral intrahippocampal injection of AβO (IH-AβO, 2 μl of 40 μM solution) performed poorly in the step-through passive avoidance test given on post-injection Day 8, compared to mice receiving bilateral intrahippocampal injections of vehicle (IH-Vehicle) only. Daily oral PAP-1 (100 mg/kg p.o.) treatment recovered this memory deficit to the control level (Fig. 5B),

Figure 2 Continued

and normalized by the amount of total cellular protein in each culture. AβO-induced NO production was reduced by PAP-1 (1 μM) or doxycycline (20 μM) treatment ($n = 3$; $^{**}P < 0.001$). (**D**) RNA was extracted for qPCR of indicated pro-inflammatory mediators (for IL-1β and TNF-α, $n = 7$; for iNOS, $n = 3$; $^{*}P < 0.05$, $^{**}P < 0.001$). (**E**) The activation state of p38 MAPK was evaluated in cell homogenates by western blot using an antibody for its phosphorylated epitope (p-p38). An antibody for p38 MAPK was used to quantify the total p38 MAPK level (t-p38). AβO (50 nM) induced a time-dependent activation of p38MAPK and this was largely abolished by PAP-1 treatment or $K_v1.3$ knockout. The cropped western blots are presented in the interest of clarity. (**F**) Cultured mouse hippocampal slices were treated with vehicle, AβO (20 nM), AβO + doxycycline (20 μM), and AβO + PAP-1 (1 μM) for 24 h, stained with Hoechst (blue) to outline the slices. Consecutive slices received the same indicated treatment. One slice was then used for PI uptake, one for Fluoro-Jade® C study for neuronal damage, one for CD11b staining for microglia activation, and one for NeuN staining for neuronal survival. AβO significantly enhanced CD11b staining, which was accompanied by neuronal damage as shown by increased PI uptake, Fluoro-Jade® C staining, and reduced NeuN staining. Microglial activation and neuronal damage were ameliorated by doxycycline and PAP-1. The locations of hippocampal subfields CA1, CA3, and dentate gyrus (DG) are indicated. (**G**) PAP-1 prevented the inhibitory effect of AβO on amplitude of hippocampal LTP induced with high frequency stimulation. The representative traces show the field excitatory postsynaptic potential (fEPSP) of baseline and at 50 min after high frequency stimulation. Slices were perfused with AβO (100 nM) for 45 min before recording, and perfused continuously throughout the recording, in the presence of PAP-1 (1 μM) or vehicle control. (**H**) Summary bar graphs showing the average fEPSP slope between 45 and 50 min after high frequency stimulation. Data were compiled from recordings using slices obtained from the groups of control (eight slices from five mice), AβO, (seven slices from three mice), PAP-1 (seven slices from five mice) and PAP-1 + AβO (eight slices from four mice). AβO alone significantly inhibited the level of hippocampal LTP and this effect was prevented by co-application of PAP-1. All data are presented as mean ± SE.

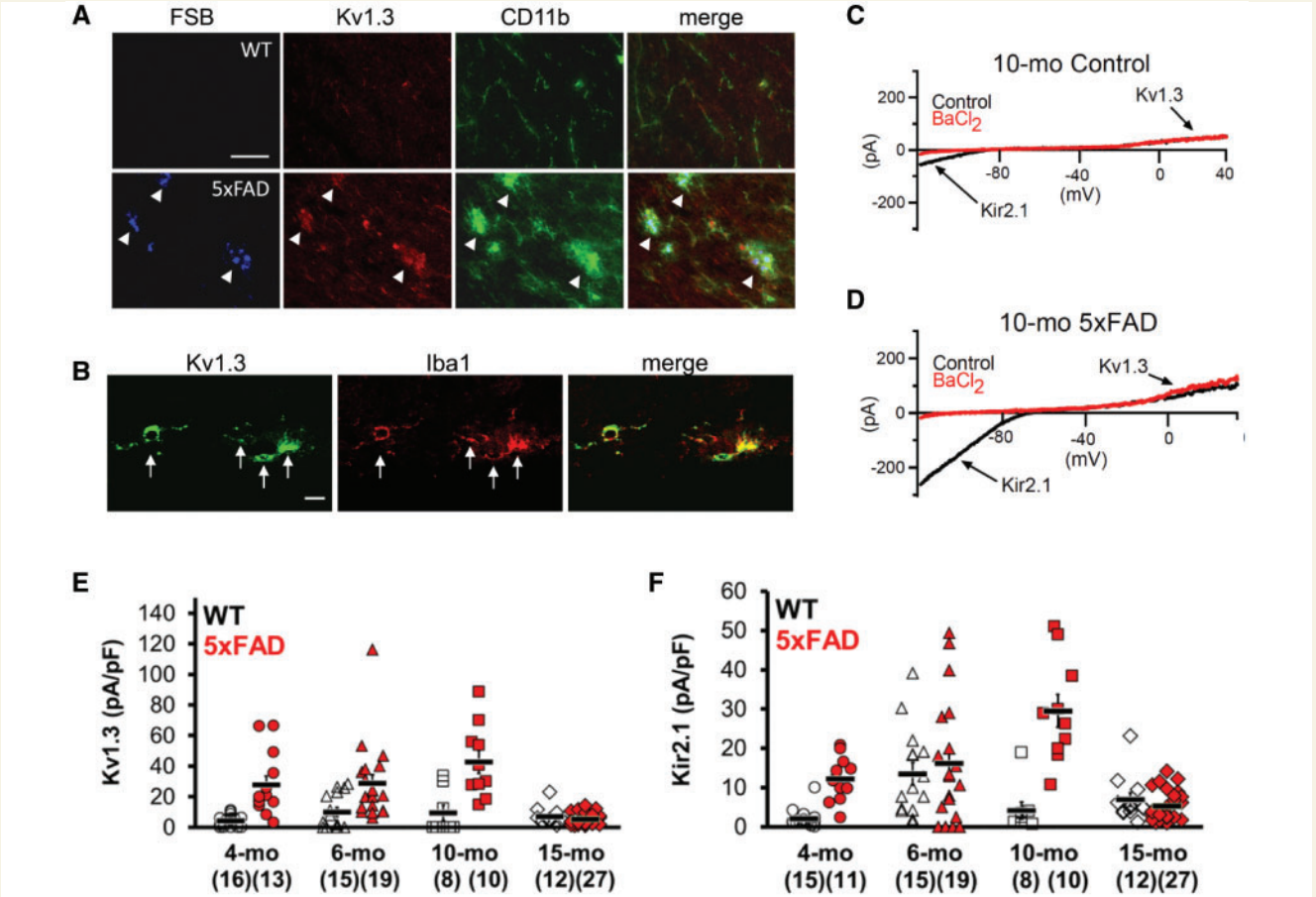

Figure 3 Microglial $K_v1.3$ expression was elevated in brains of the 5xFAD mouse model. (**A**) Corresponding coronal sections of mouse frontal cortex were fluorescently stained with the amyloid dye FSB (blue), anti-$K_v1.3$ (red), and anti-CD11b (green). $K_v1.3$ is localized to activated microglia enriched around FSB-positive amyloid plaques (white arrowheads). Scale bar = 50 μm. (**B**) Confocal images to illustration localization of $K_v1.3$ to Iba1-positive microglial cells (white arrows) in a 5xFAD brain. Scale bar = 10 μm. (**C–F**) Functional K_+ channel expression in 5xFAD microglia at different ages. Representative current traces elicited by a voltage-ramp from −120 to +40 mV from microglia from a 10-month-old wild-type (WT) control (**C**) and a 10-month-old 5xFAD mouse (**D**) showing $K_v1.3$ current at depolarized potential and BaCl2-sensitive $K_{ir}2.1$ current at hyperpolarized potential. (**E**) Current density plot showing age-dependent microglial $K_v1.3$ channel current expression in 4-month-old (wild-type = 4.13 ± 0.99 pA/pF, n = 16; 5xFAD = 27.74 ± 5.74 pA/pF, n = 13; P = 0.0001), 6-month-old (wild-type = 9.94 ± 92.971 pA/pF, n = 15; 5xFAD = 28.74 ± 5.78 pA/pF, n = 19; P = 0.0118), 10-month-old (wild-type = 9.50 ± 5.11 pA/pF, n = 8; 5xFAD = 42.81 ± 7.53 pA/pF, n = 10; P = 0.0032), and 15-month-old (wild-type = 7.00 ± 1.66 pA/pF, n = 12; 5xFAD = 5.33 ± 0.74 pA/pF, n = 27; P = 0.2920) mice. (**F**) Current density plot showing age-dependent microglial $K_{ir}2.1$ channel expression in 4-month-old (wild-type = 2.13 ± 0.63 pA/pF, n = 15; 5xFAD = 12.17 ± 1.74 pA/pF, n = 11; P = 0.000003), 6-month-old (wild-type = 13.50 ± 2.85 pA/pF, n = 15; 5xFAD = 16.14 ± 3.62 pA/pF, n = 19; P = 0.59), 10-month-old (wild-type = 4.14 ± 2.15 pA/pF, n = 8; 5xFAD = 29.51 ± 4.15 pA/pF, n = 10; P = 0.0001), and 15-month-old (wild-type = 7.00 ± 1.66 pA/pF, n = 12; 5xFAD = 5.33 ± 0.74 pA/pF, n = 27; P = 0.29) mice. Data are presented as mean ± SE and analysed using pairwise Student's t-test.

suggesting that $K_v1.3$ blockade could potentially ameliorate AβO-induced memory decline in Alzheimer's disease.

To further translate our findings into a clinically relevant context, we intended to test the effect of chronic PAP-1 treatment on the behavioural phenotype of Alzheimer's transgenic models. Unfortunately, we could not demonstrate reproducible memory deficits in 5xFAD mice at multiple ages. Therefore, we used the APP/PS1 model, which demonstrated memory deficits after 8–9 months of age, for this trial. Although compared to 5xFAD mice, APP/PS1 mice showed less robust and a later onset of Alzheimer's disease-like amyloid pathology, the microglia of APP/PS1 mice were shown to lose amyloid-β-clearing capabilities at around 8 months of age, preceding the increase in amyloid-β accumulation and coincident with the beginning of measurable behavioural deficits (Hickman *et al.*, 2008). To test if $K_v1.3$ inhibition by PAP-1 may affect the ability of microglia to clear amyloid-β, we treated cultured primary microglia with 50 nM Alexa Fluor® 488-labelled AβO and determined AβO uptake by flow cytometry. As expected, AβO uptake was reduced by an antibody 2F8 that blocks scavenger receptor A (SRA), a known microglial amyloid-β receptor (El Khoury *et al.*, 1996), and by blocking the conformational epitopes of AβO using Congo red (Maezawa

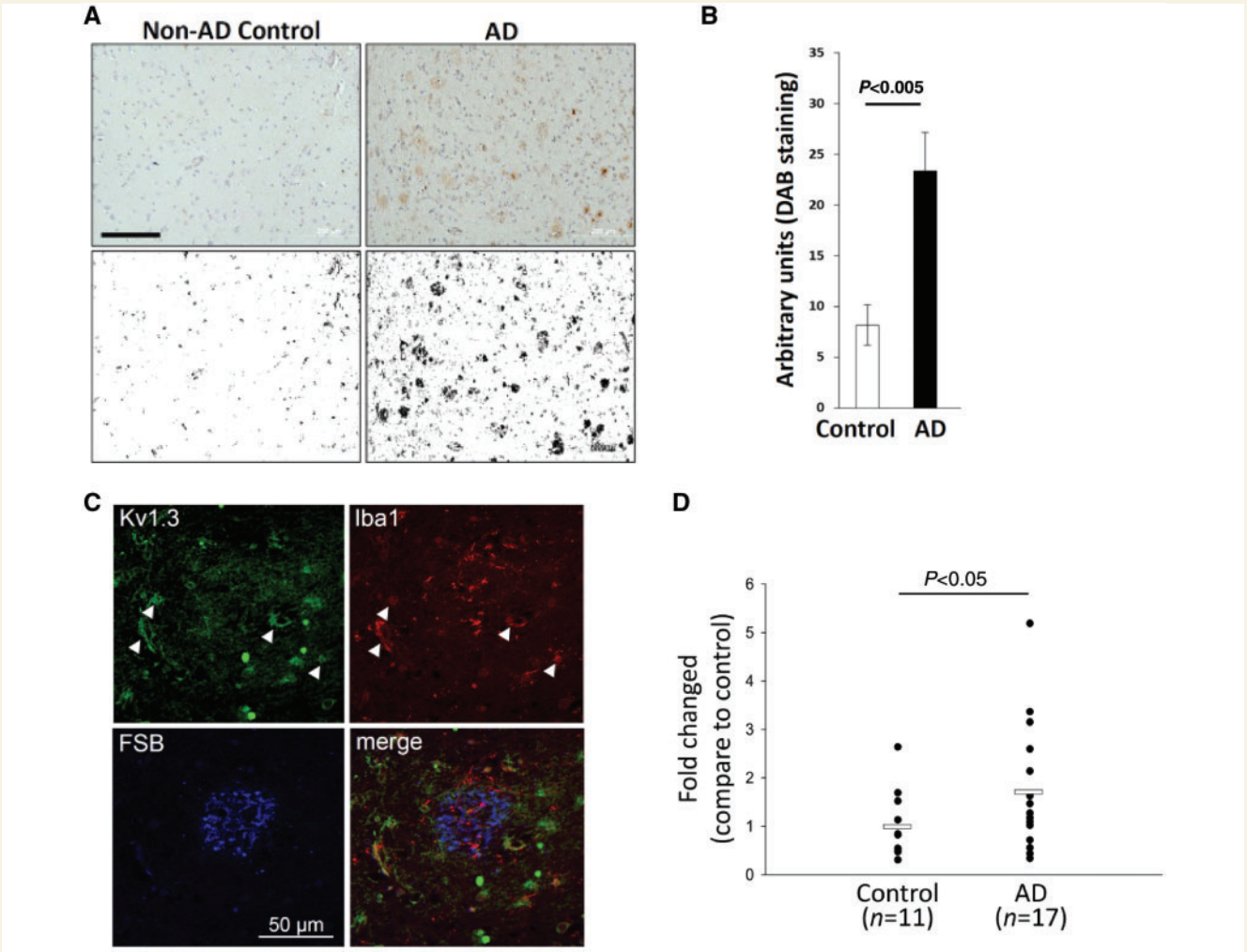

Figure 4 Increased $K_v1.3$ expression in Alzheimer's disease brains. (**A**) $K_v1.3$ expression was assessed in five Alzheimer's disease (AD) and five age-matched control brain samples from the entorhinal cortex. Shown are representative photomicrographs showing $K_v1.3$ immunoreactivities presented by diaminobenzidine (DAB). Scale bar = 200 μm. The two *lower* panels represent the same images processed for quantification using ImageJ as described in the 'Materials and methods' section. (**B**) Three random images per sample were used for analysis of DAB-positive area. $K_v1.3$ expression was increased in Alzheimer's disease hippocampus (two-tailed *t*-test). (**C**) Alzheimer's disease subjects' frontal cortex sections were fluorescently stained with FSB (blue), anti-$K_v1.3$ (green), and anti-Iba1 (red). $K_v1.3$ is localized to a majority of Iba1-immunoreactive microglia (white arrowheads) enriched around amyloid plaques. Scale bar = 50 μm. (**D**) qPCR conducted on RNA extracted from age-matched Alzheimer's disease and control frontal cortex samples showed an increased $K_v1.3$ transcript level in Alzheimer's disease subjects. Statistical analysis was conducted using two-tailed *t*-test.

et al., 2008) or an AβO-specific antibody A11 (Kayed and Glabe, 2006) (Fig. 6A). Interestingly, compared to doxycycline, a known microglia activation inhibitor, which substantially inhibited AβO uptake, PAP-1 enhanced the ability of microglia to uptake AβO (Fig. 6A). This result suggests that rather than globally suppressing microglial function, $K_v1.3$ inhibition not only preserves but may enhance the beneficial amyloid-β clearance capability. This result also suggests that PAP-1 may recover the ability of microglia to clear amyloid-β in APP/PS1 mice.

We next tested if PAP-1 affects the behavioural phenotype and amyloid deposition in APP/PS1 mice. PAP-1 was administered via *ad libitum* consumption of PAP-1-medicated diet (ppm = 1100), starting at 9 months of age for a course of 5 months. Mice receiving chronic PAP-1 treatment were well groomed and displayed no observable differences compared to wild-type littermates. PAP-1 treatment significantly improved the performance of APP/PS1 mice in novel object recognition (Fig. 6B) and step-through passive avoidance tests (Fig. 6C). The open field test showed that APP/PS1 mice had no deficits in general motor activity but had shortened centre time, which was not rectified by PAP-1 treatment (Supplementary Fig. 5), suggesting that PAP-1 does not alleviate anxiety. Immediately after conclusion of the neurobehavioural tests, brains were removed for quantification of PAP-1 levels by UPLC/MS (ultra performance liquid chromatography - tandem mass spectrometer). While mice that had

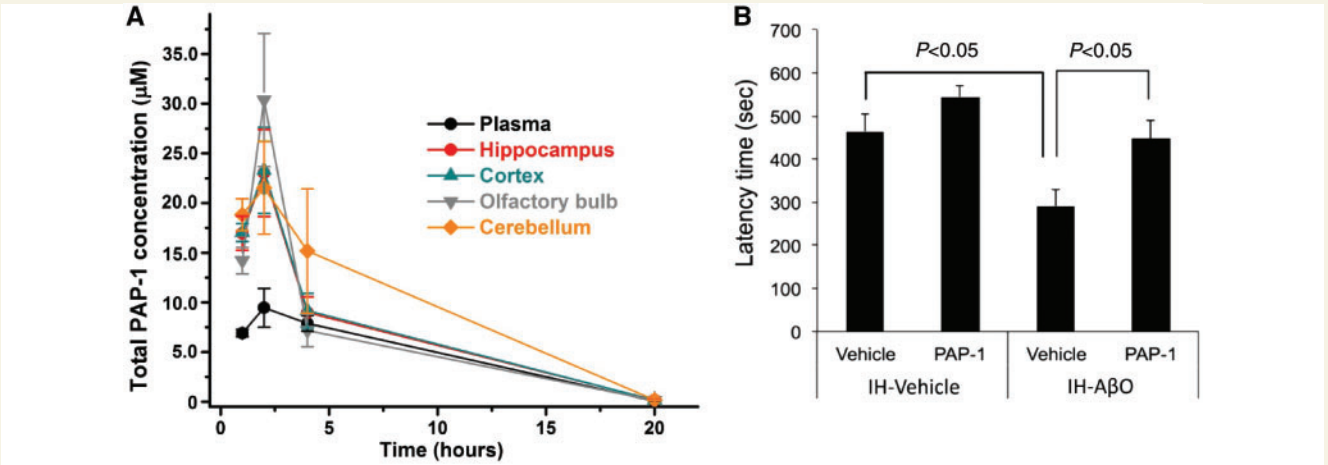

Figure 5 PAP-1 was orally available and brain penetrant, and enhanced memory performance in the IH-AβO model. (**A**) Total PAP-1 plasma and tissue concentrations in various brain regions following oral administration of 100 mg/kg PAP-1 in condensed milk ($n = 3$ mice per data point; shown are mean ± SD). (**B**) Mice having received IH-AβO or IH-Vehicle (as controls), with or without daily oral PAP-1 treatment (100 mg/kg/day), were subjected to the step-through passive avoidance test 8 days later. Mice receiving IH-AβO showed significantly shortened latency time compared to those receiving IH-Vehicle, and this deficit was mitigated in the IH-AβO mice treated with PAP-1. $n = 8$–9 per group; two-way ANOVA followed by Bonferroni *post hoc* test.

received unmedicated diet had no detectable PAP-1 levels in their brains, PAP-1-treated wild-type mice had average total brain concentrations of 608 ± 439 nM [mean ± standard deviation (SD); $n = 12$] and APP/PS1 mice concentrations of 411 ± 317 nM (mean ± SD; $n = 12$) at the time of sacrifice, demonstrating that our medicated diet regiment achieved pharmacologically active brain concentrations. PAP-1 treatment curbed microglia activation, as evidenced by reduced Iba-1 immunofluorescence (Fig. 6D) in brain sections and reduced expression of pro-inflammatory mediators in acutely isolated microglia (Supplementary Fig. 6). As expected, the level of $K_v1.3$ transcript in microglia was increased in APP/PS1 mice consuming control diet, compared to the wild-type littermates. Long-term PAP-1 treatment reduced the expression of $K_v1.3$, consistent with a reduced pro-inflammatory profile (Fig. 6E). Interestingly, PAP-1 treatment resulted in a 55% reduction of cerebral amyloid load in treated APP/PS1 mice (Fig. 6D and F). Quantities of TBS-soluble and TBS-insoluble amyloid-β in brain homogenates as determined by ELISA were also significantly reduced (Fig. 6G), consistent with the notion that $K_v1.3$ inhibition recovers the capability of microglia to clear amyloid-β *in vivo*. This notion was further strengthened by the observation that PAP-1 treatment also reduced the amyloid load as well as microglial activation in 5xFAD mice (Supplementary Fig. 7). Furthermore, PAP-1 treatment rectified the hippocampal LTP deficit in APP/PS1 mice to the wild-type level (Fig. 6H and I), consistent with the improved memory performance.

Discussion

Several key conclusions can be drawn from our study: (i) soluble AβO, the highly toxic amyloid-β species implicated as one of the principal initiators of Alzheimer's disease phenotypes (Selkoe and Hardy, 2016), enhances microglial $K_v1.3$ and $K_{ir}2.1$ activity, two K^+ channels characteristic of LPS- and IL-4-induced microglial polarization, respectively; (ii) $K_v1.3$ is required for AβO-induced microglial pro-inflammatory activation and neurotoxicity; (iii) $K_v1.3$ expression/activity is upregulated in transgenic Alzheimer's disease animals and human Alzheimer's disease brains; and (iv) pharmacological inhibition of $K_v1.3$ with PAP-1 in mice mitigates some key Alzheimer's disease-like phenotypes including memory deficit and amyloid pathology. Our study suggests that $K_v1.3$ is a candidate therapeutic target for Alzheimer's disease and that our selective small molecule $K_v1.3$ inhibitor PAP-1 is a promising therapeutic agent. The observations that pharmacological targeting of microglial $K_v1.3$ channels can affect hippocampal synaptic plasticity and reduce amyloid deposition in APP/PS1 mice are particularly interesting and support the potential of neuro-immunomodulation in treating neurodegenerative disorders (Marin and Kipnis, 2017).

When stimulating microglia *in vitro* we previously found that increased $K_v1.3$ expression was characteristic of LPS-induced 'M1-like' polarization, while expression of the inward-rectifier $K_{ir}2.1$ was a feature of IL-4-induced 'M2-like' polarization (Nguyen *et al.*, 2017). This is reminiscent of our previous finding that different T and B cell subsets significantly differ in their K^+ channel expression profile. For example, $CCR7^-$ effector memory T cells and IgD^-CD27^+ B cells upregulate $K_v1.3$ and rely on this channel for their Ca^{2+} signalling, while $CCR7^+$ naïve and central memory T cells as well as IgD^+ B cells upregulate a different K^+ channel after activation, the calcium-activated $K_{Ca}3.1$ channel (Wulff *et al.*, 2003, 2004; Beeton *et al.*, 2006). However, in contrast to cells of the adaptive

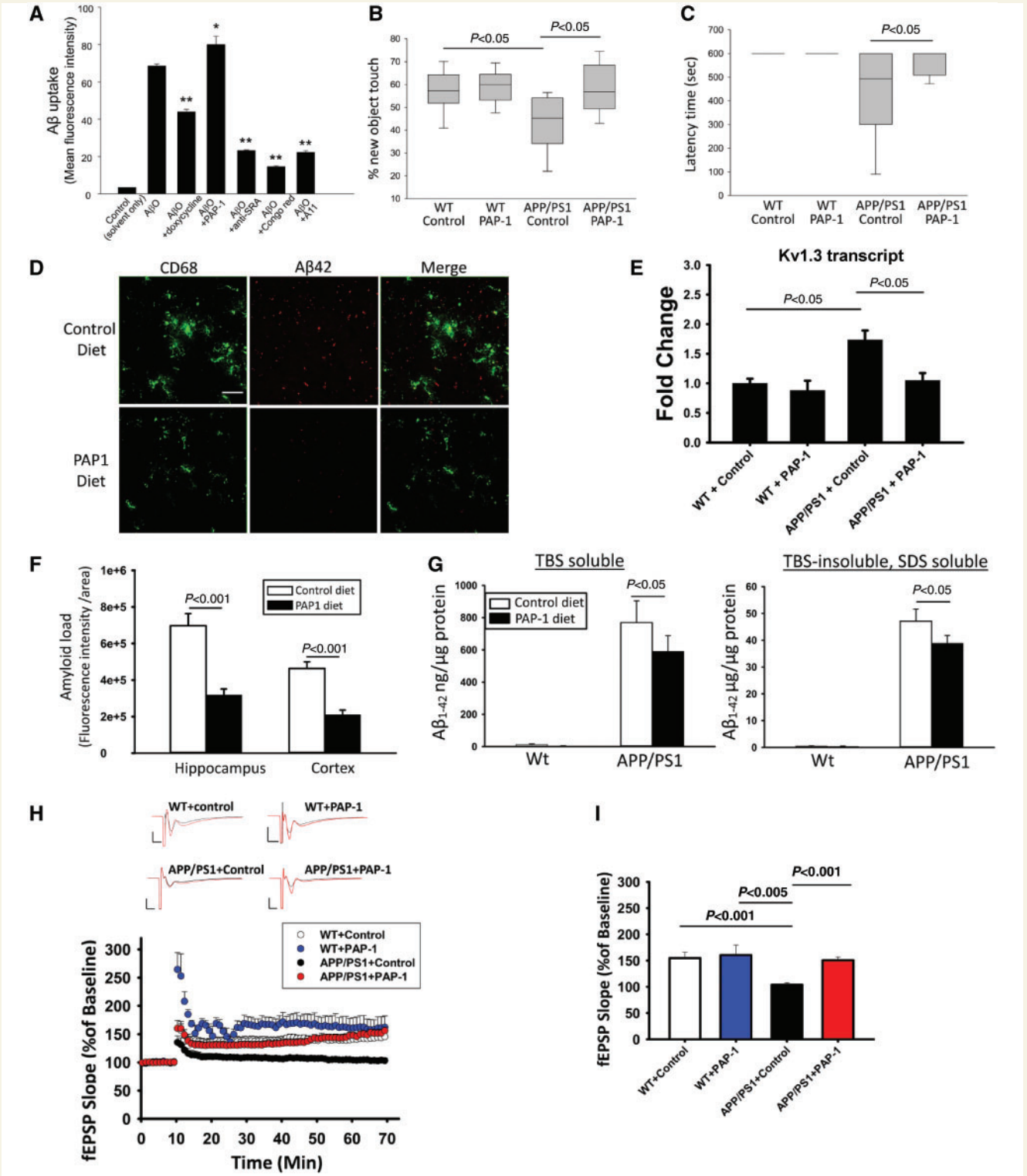

Figure 6 Chronic oral administration of PAP-1 to APP/PS1 mice ameliorated the hippocampal LTP and memory deficits and reduced the amyloid load. (**A**) Uptake of fluorescently-labelled AβO (50 nM, 1 h incubation) by cultured microglia. PAP-1 (1 μM), in contrast to doxycycline (20 μM), enhanced the ability of microglia to uptake AβO. $n = 3$; one-way ANOVA with Bonferroni multiple comparisons versus control (AβO only) group; $^*P < 0.05$ and $^{**}P < 0.001$. (**B–I**) Four groups of mice were treated with assigned diet from age 9 to 14 months: wild-type/control diet ($n = 10$), wild-type/PAP-1 diet ($n = 13$), APP/PS1/control diet ($n = 9$), and APP/PS1/PAP-1 diet ($n = 11$). Data were analysed by two-way ANOVA follow by Bonferroni *post hoc* test. (**B** and **C**) Near the conclusion of the treatment, cognitive abilities were tested by novel object recognition and step-through passive avoidance tests. The box plots show the median and 25% and 75% interquartile range. APP/PS1 mice on control diet failed to exhibit novel object recognition, but this deficit was mitigated by PAP-1 diet (**B**). Likewise, APP/PS1 mice on control diet exhibited shortened median latency time in the passive avoidance test, which was significantly lengthened by PAP-1 diet (**C**). (**D–I**) The brains

(continued)

immune system, which acquire stable phenotypes after subtype differentiation or class-switching, cells of the innate immune system such as microglia are highly plastic and typically do not acquire a stable phenotype that can be readily categorized by specific markers or signature genes (Murray *et al.*, 2014; Bohlen *et al.*, 2017). The M1/M2 classification defined by a set of markers is therefore considered an oversimplification and could be a misleading characterization of microglia activation *in vivo* (Ransohoff, 2016). In this study, based on not only *in vitro* but also *in vivo* data, we concluded that microglial $K_v1.3$ expression/activity is enhanced by AβO, and is required for AβO-induced microglial pro-inflammatory responses and associated neurotoxicity. Amyloid-β aggregates, including AβO, stimulate microglia in part via a well-known LPS receptor, TLR4 (Toll-like receptor 4) (Capiralla *et al.*, 2012; Ledo *et al.*, 2016), and induce responses widely considered as pro-inflammatory. However, AβO, differing from LPS, induced enhancement of both $K_v1.3$ and $K_{ir}2.1$ current density. Moreover, our studies using whole-cell patch-clamp recording, a single-cell approach, clearly showed that $K_v1.3$ and $K_{ir}2.1$ were co-expressed in single AβO-treated microglia, rather than segregated into different cell populations. AβO treatment also induced simultaneous expressions of markers traditionally used to categorize M1 and M2 polarization. This result is consistent with a previous single-cell gene expression study showing that individual myeloid cells responding to traumatic brain injury concurrently adopted both inflammatory and reparative features with a lack of exclusivity (Kim *et al.*, 2016; Ransohoff, 2016) and suggests that AβO-treated microglia adopted an activation state that is more complex than simply being 'pro-inflammatory' or 'neurotoxic', and may even entail some M2-like tissue repair activity.

The age-dependent changes in microglial $K_v1.3$ and $K_{ir}2.1$ expression in 5xFAD mice followed a similar trend—initially an age-dependent increase, then a substantial decrease between 10 and 15 months of age. We suspect that these changes in K^+ channel expression form part of the age-related changes in microglial function, documented by several lines of investigation, such as altered responses to amyloid-β aggregates or downregulation of 'sensome' genes (Hickman *et al.*, 2008, 2013; Cameron *et al.*, 2012; Heneka *et al.*, 2013; Johansson *et al.*, 2015). Our findings may also reflect the age-associated microglial dysfunction observed in mouse models overproducing amyloid-β (Hickman *et al.*, 2008; Cameron *et al.*, 2012; Heneka *et al.*, 2013). However, the downregulation of $K_v1.3$ was not observed in human brains with advanced Alzheimer's disease pathologies, in which $K_v1.3$ expression remains quite robust in microglia, especially in those associated with amyloid plaques (Fig. 4) (Rangaraju *et al.*, 2015). This result suggests that current transgenic models of Alzheimer's disease do not completely replicate the patterns of microglia activation in human Alzheimer's disease, in which multiple stimuli other than amyloid-β may mould the eventual microglial phenotypes. In any case, the human study supports that $K_v1.3$ could be a therapeutic target even at the late stage.

While in wild-type mice the basal levels of $K_v1.3$ and $K_{ir}2.1$ remained low, the $K_{ir}2.1$ level was high as measured at 6 months (Fig. 3E), suggesting an unknown physiological function in adult microglia. Although some extrapolation can be made from a previous study implicating $K_{ir}2.1$ activity in microglial Ca^{2+} signalling and migration under 'resting' and 'anti-inflammatory states' (Lam and Schlichter, 2015) and our own study showing that IL-4 induces large $K_{ir}2.1$ currents (Nguyen *et al.*, 2017), these studies were performed on cultured neonatal microglia. In contrast to $K_v1.3$, an important limitation preventing us from gaining insight into the *in vivo* role of $K_{ir}2.1$ is a lack of good pharmacological or genetic tools to analyse the significance of AβO-induced $K_{ir}2.1$ upregulation in microglia in adult and aged mice. $K_{ir}2.1$ plays a vital role in the vasculature and in cardiac excitability; its knockout causes mice to die within hours after birth (Zaritsky *et al.*, 2001). The only available $K_{ir}2.1$ inhibitors, high micromolar to millimolar Ba^{2+} or the small molecule ML133 (IC_{50} 2 μM) (Wang *et al.*, 2011), are both unsuitable for *in vivo* use and are even problematic in experiments with cultured microglia because of their high toxicity (Nguyen *et al.*, 2017). Future developments of mice with microglia-targeted deletion of $K_{ir}2.1$ and specific, non-toxic $K_{ir}2.1$ inhibitors are required to illuminate the *in vivo* role of microglial $K_{ir}2.1$ in Alzheimer's disease.

It is intriguing to hypothesize that selectively blocking microglial $K_v1.3$ activity without affecting $K_{ir}2.1$ function would mitigate the neurotoxicity accompanying the pro-inflammatory activation while preserving the anti-inflammatory and tissue repair functions associated with IL-4-like

Figure 6 Continued

were removed for immunohistochemistry, amyloid-β quantification, and electrophysiological recording. Frontal cortex sections co-stained with CD68 and amyloid-β_{42} showed that PAP-1 diet reduced the CD68 and amyloid-β reactivities in APP/PS1 brains (**D**, shown are representative confocal images, scale bar = 50 μm). The level of $K_v1.3$ transcript in acutely isolated microglia was increased in APP/PS1 mice consuming control diet, compared to the wild-type littermates. PAP-1 diet reduced the expression of $K_v1.3$ (**E**). Quantification of five consecutive sections from each animal showed that PAP-1 diet significantly reduced FSB-reactive fibrillary amyloid in both hippocampus and frontal cortex (**F**). The fresh brains were fractionated into TBS-soluble and TBS-insoluble, SDS-soluble fractions, which were used for ELISA quantification of amyloid-β_{42}. PAP-1 diet significantly reduced the levels of amyloid-β_{42} in both fractions (**G**). (**H**) Traces and time course of hippocampal LTP induced with high frequency stimulation. (**I**) Summary bar graphs showing the average fEPSP slope between 50 and 60 min, compiled from recordings of wild-type/control (10 slices from three mice), wild-type/PAP-1 (four slices from two mice), APP/PS1/control (12 slices from three mice), and APP/PS1/PAP-1 (12 slices from three mice). APP/PS1 mice on control diet had reduced amplitudes of hippocampal LTP but this reduction was mitigated by PAP-1 diet.

effects. Indeed, our data using pharmacological $K_v1.3$ targeting are consistent with the above hypothesis, and support $K_v1.3$ blockers as attractive therapeutic agents to mitigate amyloid-β-induced pro-inflammatory microglial responses that are highly relevant to Alzheimer's disease pathogenesis (Go *et al.*, 2016; Ledo *et al.*, 2016; Rangaraju *et al.*, 2017). Furthermore, the parallel hyperexpression of microglial $K_v1.3$ in transgenic Alzheimer's disease mouse models and in human Alzheimer's disease brain tissue validates $K_v1.3$ as a therapeutic target for Alzheimer's disease and/or mild cognitive impairment preceding Alzheimer's disease.

The significance of microglia in modulating Alzheimer's disease-like amyloid pathology remains controversial. Our *in vitro* data presented in Fig. 6A and *in vivo* data of substantial reductions of cerebral soluble and insoluble amyloid-β species in mice chronically treated with PAP-1 (Fig. 6D–G and Supplementary Fig. 7) suggest that $K_v1.3$ inhibition enhances the microglial amyloid-β clearance capacity that is suppressed in Alzheimer's disease transgenic mice (Hickman *et al.*, 2008; Hellwig *et al.*, 2015). On the other hand, reductions of pro-inflammatory cytokines, as a result of $K_v1.3$ blockade, might also lead to decreased cerebral amyloid-β levels (Tan *et al.*, 2014). Our result is consistent with several reports showing that selective modulation of specific microglial signalling pathways alters amyloid-β deposition and clearance (El Khoury *et al.*, 2007; Cameron *et al.*, 2012; Heneka *et al.*, 2013; Guillot-Sestier *et al.*, 2015; Hellwig *et al.*, 2015; Johansson *et al.*, 2015; Krauthausen *et al.*, 2015), but appears contradictory to reports showing that inducible microglia depletion by genetic or pharmacological means fails to affect amyloid pathology in transgenic Alzheimer's disease models (Grathwohl *et al.*, 2009; Spangenberg *et al.*, 2016). Although further studies are needed to resolve this controversy, our data using K^+ channel expression as a readout show that the microglial activation profiles in transgenic Alzheimer's disease mice are complex and age-dependent, as discussed above. Therefore, differences in the timing and approaches of neuro-immunomodulation to alter microglia quantity or signalling may differentially influence the outcomes. In our experiments, PAP-1 was administered to APP/PS1 mice at an age when microglia amyloid-β clearance capacity was impaired (Hickman *et al.*, 2008). We hypothesize that while eliminating microglia at this stage may not alter the amyloid-β homeostasis as they cease to function properly, interventions to 'rehabilitate' the phagocytic capacity of existing microglia will reduce amyloid-β deposition (Guillot-Sestier *et al.*, 2015). Our data suggest that $K_v1.3$ inhibition could be a means for such rehabilitation.

One limitation of the current study is that we cannot completely exclude the possible contributions of peripheral monocyte-derived macrophages and effector memory T cells, which also express $K_v1.3$ (Wulff *et al.*, 2003; Feske *et al.*, 2015). Peripheral immune modulation may impact neuroinflammation or brain function via humoral or cellular factors (Villeda *et al.*, 2014; Prinz and Priller, 2017). While it remains controversial whether there is an influx of peripheral immune cells into the brain in Alzheimer's disease mouse models or in human Alzheimer's disease brains (Bien-Ly *et al.*, 2015; Prinz and Priller, 2017), many brain mononuclear phagocytes that surround amyloid-β plaques are $CD45^{high}$, suggesting their peripheral monocyte origin (Jay *et al.*, 2015). Several groups also reported the presence of T cells in the brain of Alzheimer's disease patients (Itagaki *et al.*, 1988; Town *et al.*, 2005; Bryson and Lynch, 2016). Myeloid cells and lymphocytes were also found in the newly identified meningeal lymphatics (Louveau *et al.*, 2015), through which the trafficking of immune cells might influence brain pathology. It is important in future studies to use *Cre* recombinase-guided cell targeting to selectively knockout $K_v1.3$ in brain microglia, peripheral macrophages/monocytes, or T cells, in order to parse out their relative contributions to Alzheimer's disease pathogenesis. Although the current study does not distinguish the respective contribution of peripheral immune cells and brain myeloid cells, this limitation, nonetheless, does not hamper the translational potential of $K_v1.3$ blockers in Alzheimer's disease therapy.

For future clinical development, one may raise the concern that inhibiting $K_v1.3$ may make individuals susceptible to infection or cause immune dysregulation. However, in contrast to stronger immunosuppressants like calcineurin inhibitors and anti-TNF reagents, $K_v1.3$ inhibitors are 'mild' immunosuppressants and do not affect the ability of rodents or primates to clear bacterial or viral infections (Pereira *et al.*, 2007; Matheu *et al.*, 2008). Overall, $K_v1.3$ is regarded as a relatively safe drug target (Wulff *et al.*, 2009). PAP-1 does not prevent rhesus macaques from developing a protective, central memory T cell response following intranasal application of a flu vaccine (Pereira *et al.*, 2007). *Kcna3*/$K_v1.3^{-/-}$ mice are viable, reproduce normally and exhibit very subtle phenotypes (Koni *et al.*, 2003; Fadool *et al.*, 2004). Toxicity studies with PAP-1 and the peptidic $K_v1.3$ blocker ShK-186 have so far not revealed any toxicity despite 6 months or 28 days of continuous administration in rats or rhesus macaques (Beeton *et al.*, 2006; Pereira *et al.*, 2007; Tarcha *et al.*, 2012). PAP-1 has further completed IND (Investigational New Drug)-enabling toxicity studies, while ShK-186 has passed both IND toxicity studies and phase 1 safety studies without any adverse findings and has demonstrated efficacy in a small phase 1b study in plaque psoriasis (Tarcha *et al.*, 2017). The current study, showing excellent brain penetrance, no apparent toxicity after chronic treatment, and satisfactory efficacy, provides necessary proof-of-concept data to advance $K_v1.3$ blockers such as PAP-1 to clinical trials on Alzheimer's disease and/or mild cognitive impairment.

Funding

This work was supported by a grant from the Alzheimer's Association NIRG-10-174150 to I.M., the U.S. NIH grants

R21 AG038910 (NIA) to L-W.J., and R01 NS098328 (NINDS) to H.W., and in part by R01 AG043788 to I.M., P30 AG10129 to L-W.J., K08 NS099474 to S.R., P30 NS055077 (NINDS) and P50 AG025688 (NIA) to A.I.L, and U54 HD079125 to K.K. The content is solely the responsibility of the authors and does not necessarily represent the official views of the National Institutes of Health.

Supplementary material

Supplementary material is available at *Brain* online.

References

Beeton C, Wulff H, Standifer NE, Azam P, Mullen KM, Pennington MW, et al. Kv1.3 channels are a therapeutic target for T cell-mediated autoimmune diseases. Proc Natl Acad Sci USA 2006; 103: 17414–19.

Bien-Ly N, Boswell CA, Jeet S, Beach TG, Hoyte K, Luk W, et al. Lack of widespread BBB disruption in Alzheimer's disease models: focus on therapeutic antibodies. Neuron 2015; 88: 289–97.

Bohlen CJ, Bennett FC, Tucker AF, Collins HY, Mulinyawe SB, Barres BA. Diverse requirements for microglial sSurvival, specification, and function revealed by defined-medium cultures. Neuron 2017; 94: 759–73.e8.

Bryson KJ, Lynch MA. Linking T cells to Alzheimer's disease: from neurodegeneration to neurorepair. Curr Opin Pharmacol 2016; 26: 67–73.

Cameron B, Tse W, Lamb R, Li X, Lamb BT, Landreth GE. Loss of interleukin receptor-associated kinase 4 signaling suppresses amyloid pathology and alters microglial phenotype in a mouse model of Alzheimer's disease. J Neurosci 2012; 32: 15112–23.

Capiralla H, Vingtdeux V, Zhao HT, Sankowski R, Al-Abed Y, Davies P, et al. Resveratrol mitigates lipopolysaccharide- and A ss-mediated microglial inflammation by inhibiting the TLR4/NF-κB/STAT signaling cascade. J Neurochem 2012; 120: 461–72.

Chandy KG, Wulff H, Beeton C, Pennington M, Gutman GA, Cahalan MD. Potassium channels as targets for specific immunomodulation. Trends Pharmacol Sci 2004; 25: 280–9.

Chen YJ, Nguyen HM, Maezawa I, Grossinger EM, Garing AL, Kohler R, et al. The potassium channel KCa3.1 constitutes a pharmacological target for neuroinflammation associated with ischemia/reperfusion stroke. J Cereb Blood Flow Metab 2016; 36: 2146–61.

El Khoury J, Hickman SE, Thomas CA, Cao L, Silverstein SC, Loike JD. Scavenger receptor-mediated adhesion of microglia to β-amyloid fibrils. Nature 1996; 382: 716–19.

El Khoury J, Toft M, Hickman SE, Means TK, Terada K, Geula C, et al. Ccr2 deficiency impairs microglial accumulation and accelerates progression of Alzheimer-like disease. Nat Med 2007; 13: 432–8.

Fadool DA, Tucker K, Perkins R, Fasciani G, Thompson RN, Parsons AD, et al. Kv1.3 channel gene-targeted deletion produces "Super-Smeller Mice" with altered glomeruli, interacting scaffolding proteins, and biophysics. Neuron 2004; 41: 389–404.

Feske S, Wulff H, Skolnik EY. Ion channels in innate and adaptive immunity. Annu Rev Immunol 2015; 33: 291–353.

Fordyce CB, Jagasia R, Zhu X, Schlichter LC. Microglia Kv1.3 channels contribute to their ability to kill neurons. J Neurosci 2005; 25: 7139–49.

Garciacalvo M, Leonard RJ, Novick J, Stevens SP, Schmalhofer W, Kaczorowski GJ, et al. Purification, characterization, and biosynthesis of margatoxin, a component of Centruroides-Margaritatus venom that selectively inhibits voltage-dependent potassium channels. J Biol Chem 1993; 268: 18866–74.

Go M, Kou JH, Lim JE, Yang JL, Fukuchi KI. Microglial response to LPS increases in wild-type mice during aging but diminishes in an Alzheimer's mouse model: implication of TLR4 signaling in disease progression. Biochem Biophys Res Commun 2016; 479: 331–7.

Grathwohl SA, Kalin RE, Bolmont T, Prokop S, Winkelmann G, Kaeser SA, et al. Formation and maintenance of Alzheimer's disease beta-amyloid plaques in the absence of microglia. Nat Neurosci 2009; 12: 1361–3.

Griffin MO, Fricovsky E, Ceballos G, Villarreal F. Tetracyclines: a pleitropic family of compounds with promising therapeutic properties. Review of the literature. Am J Physiol Cell Physiol 2010; 299: C539–48.

Guillot-Sestier MV, Doty KR, Gate D, Rodriguez J Jr, Leung BP, Rezai-Zadeh K, et al. Il10 deficiency rebalances innate immunity to mitigate Alzheimer-like pathology. Neuron 2015; 85: 534–48.

Hellwig S, Masuch A, Nestel S, Katzmarski N, Meyer-Luehmann M, Biber K. Forebrain microglia from wild-type but not adult 5xFAD mice prevent amyloid-beta plaque formation in organotypic hippocampal slice cultures. Sci Rep 2015; 5: 14624.

Helms LM, Felix JP, Bugianesi RM, Garcia ML, Stevens S, Leonard RJ, et al. Margatoxin binds to a homomultimer of K(V)1.3 channels in Jurkat cells. Comparison with K(V)1.3 expressed in CHO cells. Biochemistry 1997; 36: 3737–44.

Heneka MT, Carson MJ, El Khoury J, Landreth GE, Brosseron F, Feinstein DL, et al. Neuroinflammation in Alzheimer's disease. Lancet Neurol 2015; 14: 388–405.

Heneka MT, Kummer MP, Stutz A, Delekate A, Schwartz S, Vieira-Saecker A, et al. NLRP3 is activated in Alzheimer's disease and contributes to pathology in APP/PS1 mice. Nature 2013; 493: 674–8.

Hickman SE, Allison EK, El Khoury J. Microglial dysfunction and defective beta-amyloid clearance pathways in aging Alzheimer's disease mice. J Neurosci 2008; 28: 8354–60.

Hickman SE, Kingery ND, Ohsumi TK, Borowsky ML, Wang LC, Means TK, et al. The microglial sensome revealed by direct RNA sequencing. Nat Neurosci 2013; 16: 1896–905.

Hong HS, Maezawa I, Yao N, Xu B, Diaz-Avalos R, Rana S, et al. Combining the rapid MTT formazan exocytosis assay and the MC65 protection assay led to the discovery of carbazole analogs as small molecule inhibitors of Abeta oligomer-induced cytotoxicity. Brain Res 2007; 1130: 223–34.

Hong HS, Rana S, Barrigan L, Shi A, Zhang Y, Zhou F, et al. Inhibition of Alzheimer's amyloid toxicity with a tricyclic pyrone molecule *in vitro* and *in vivo*. J Neurochem 2009; 108: 1097–108.

Horiuchi M, Smith L, Maezawa I, Jin LW. CX3CR1 ablation ameliorates motor and respiratory dysfunctions and improves survival of a Rett syndrome mouse model. Brain Behav Immun 2017; 60: 106–16.

Itagaki S, McGeer PL, Akiyama H. Presence of T-cytotoxic suppressor and leucocyte common antigen positive cells in Alzheimer's disease brain tissue. Neurosci Lett 1988; 91: 259–64.

Jankowsky JL, Fadale DJ, Anderson J, Xu GM, Gonzales V, Jenkins NA, et al. Mutant presenilins specifically elevate the levels of the 42 residue beta-amyloid peptide *in vivo*: evidence for augmentation of a 42-specific gamma secretase. Hum Mol Genet 2004; 13: 159–70.

Jay TR, Miller CM, Cheng PJ, Graham LC, Bemiller S, Broihier ML, et al. TREM2 deficiency eliminates TREM2+ inflammatory macrophages and ameliorates pathology in Alzheimer's disease mouse models. J Exp Med 2015; 212: 287–95.

Jin LW, Horiuchi M, Wulff H, Liu XB, Cortopassi GA, Erickson JD, et al. Dysregulation of glutamine transporter SNAT1 in Rett syndrome microglia: a mechanism for mitochondrial dysfunction and neurotoxicity. J Neurosci 2015; 35: 2516–29.

Johansson JU, Woodling NS, Wang Q, Panchal M, Hang XB, Trueba-Saiz A, et al. Prostaglandin signaling suppresses beneficial microglial

function in Alzheimer's disease models. J Clin Invest 2015; 125: 350–64.
Karch CM, Cruchaga C, Goate AM. Alzheimer's disease genetics: from the bench to the clinic. Neuron 2014; 83: 11–26.
Kayed R, Glabe CG. Conformation-dependent anti-amyloid oligomer antibodies. Methods Enzymol 2006; 413: 326–44.
Kettenmann H, Hanisch UK, Noda M, Verkhratsky A. Physiology of microglia. Physiol Rev 2011; 91: 461–553.
Kim CC, Nakamura MC, Hsieh CL. Brain trauma elicits non-canonical macrophage activation states. J Neuroinflammation 2016; 13: 117.
Koni PA, Khanna R, Chang MC, Tang MD, Kaczmarek LK, Schlichter LC, et al. Compensatory anion currents in Kv1.3 channel-deficient thymocytes. J Biol Chem 2003; 278: 39443–51.
Krauthausen M, Kummer MP, Zimmermann J, Reyes-Irisarri E, Terwel D, Bulic B, et al. CXCR3 promotes plaque formation and behavioral deficits in an Alzheimer's disease model. J Clin Invest 2015; 125: 365–78.
Kundu-Raychaudhuri S, Chen YJ, Wulff H, Raychaudhuri SP. Kv1.3 in psoriatic disease: PAP-1, a small molecule inhibitor of Kv1.3 is effective in the SCID mouse psoriasis - Xenograft model. J Autoimmun 2014; 55: 63–72.
Lam D, Schlichter LC. Expression and contributions of the Kir2.1 inward-rectifier K(+) channel to proliferation, migration and chemotaxis of microglia in unstimulated and anti-inflammatory states. Front Cell Neurosci 2015; 9: 185.
Lambert MP, Barlow AK, Chromy BA, Edwards C, Freed R, Liosatos M, et al. Diffusible, nonfibrillar ligands derived from Aβ1-42 are potent central nervous system neurotoxins. Proc Natl Acad Sci USA 1998; 95: 6448–53.
Ledo JH, Azevedo EP, Beckman D, Ribeiro FC, Santos LE, Razolli DS, et al. Cross talk between brain innate immunity and serotonin signaling underlies depressive-like behavior induced by Alzheimer's amyloid-β oligomers in mice. J Neurosci 2016; 36: 12106–16.
Louveau A, Smirnov I, Keyes TJ, Eccles JD, Rouhani SJ, Peske JD, et al. Structural and functional features of central nervous system lymphatic vessels. Nature 2015; 523: 337–41.
Maezawa I, Hong HS, Liu R, Wu CY, Cheng RH, Kung MP, et al. Congo red and thioflavin-T analogs detect Aβ oligomers. J Neurochem 2008; 104: 457–68.
Maezawa I, Hong HS, Wu HC, Battina SK, Rana S, Iwamoto T, et al. A novel tricyclic pyrone compound ameliorates cell death associated with intracellular amyloid-β oligomeric complexes. J Neurochem 2006; 98: 57–67.
Maezawa I, Zimin PI, Wulff H, Jin LW. Amyloid-β protein oligomer at low nanomolar concentrations activates microglia and induces microglial neurotoxicity. J Biol Chem 2011; 286: 3693–706.
Maezawa I, Zou B, Di Lucente J, Cao W, Pascual C, Weerasekara S, et al. The Anti-Aβ and neuroprotective properties of a novel tricyclic pyrone molecule. J Alzheimers Dis 2017; 58: 559–74.
Marin IA, Kipnis J. Central nervous system: (immunological) ivory tower or not? Neuropsychopharmacol 2017; 42: 28–35.
Matheu MP, Beeton C, Garcia A, Chi V, Rangaraju S, Safrina O, et al. Imaging of effector memory T cells during a delayed-type hypersensitivity reaction and suppression by Kv1.3 channel block. Immunity 2008; 29: 602–14.
Murray PJ, Allen JE, Biswas SK, Fisher EA, Gilroy DW, Goerdt S, et al. Macrophage activation and polarization: nomenclature and experimental guidelines. Immunity 2014; 41: 14–20.
Nguyen HM, Grossinger EM, Horiuchi M, Davis KW, Jin LW, Maezawa I, et al. Differential Kv1.3, KCa3.1, and Kir2.1 expression in "classically" and "alternatively" activated microglia. Glia 2017; 65: 106–21.
Oakley H, Cole SL, Logan S, Maus E, Shao P, Craft J, et al. Intraneuronal beta-amyloid aggregates, neurodegeneration, and neuron loss in transgenic mice with five familial Alzheimer's disease mutations: potential factors in amyloid plaque formation. J Neurosci 2006; 26: 10129–40.
Peng Y, Lu K, Li Z, Zhao Y, Wang Y, Hu B, et al. Blockade of Kv1.3 channels ameliorates radiation-induced brain injury. Neuro Oncol 2014; 16: 528–39.
Pereira LE, Villinger F, Wulff H, Sankaranarayanan A, Raman G, Ansari AA. Pharmacokinetics, toxicity, and functional studies of the selective Kv1.3 channel blocker 5-(4-phenoxybutoxy)psoralen in rhesus macaques. Exp Biol Med 2007; 232: 1338–54.
Prinz M, Priller J. The role of peripheral immune cells in the CNS in steady state and disease. Nat Neurosci 2017; 20: 136–44.
Rangaraju S, Gearing M, Jin LW, Levey A. Potassium channel Kv1.3 is highly expressed by microglia in human Alzheimer's disease. J Alzheimers Dis 2015; 44: 797–808.
Rangaraju S, Raza SA, Pennati A, Deng Q, Dammer EB, Duong D, et al. A systems pharmacology-based approach to identify novel Kv1.3 channel-dependent mechanisms in microglial activation. J Neuroinflammation 2017; 14: 128.
Ransohoff RM. A polarizing question: do M1 and M2 microglia exist? Nat Neurosci 2016; 19: 987–91.
Rogers J. The inflammatory response in Alzheimer's disease. J Periodontol 2008; 79 (Suppl 8): 1535–43.
Schmitz A, Sankaranarayanan A, Azam P, Schmidt-Lassen K, Homerick D, Hansel W, et al. Design of PAP-1, a selective small molecule Kv1.3 blocker, for the suppression of effector memory T cells in autoimmune diseases. Mol Pharmacol 2005; 68: 1254–70.
Selkoe DJ, Hardy J. The amyloid hypothesis of Alzheimer's disease at 25 years. EMBO Mol Med 2016; 8: 595–608.
Seyfried NT, Dammer EB, Swarup V, Nandakumar D, Duong DM, Yin L, et al. A multi-network approach identifies protein-specific co-expression in asymptomatic and symptomatic Alzheimer's disease. Cell Syst 2017; 4: 60–72.e4.
Spangenberg EE, Lee RJ, Najafi AR, Rice RA, Elmore MRP, Blurton-Jones M, et al. Eliminating microglia in Alzheimer's mice prevents neuronal loss without modulating amyloid-beta pathology. Brain 2016; 139: 1265–81.
Tan MS, Yu JT, Jiang T, Zhu XC, Guan HS, Tan L. IL12/23 p40 inhibition ameliorates Alzheimer's disease-associated neuropathology and spatial memory in SAMP8 mice. J Alzheimers Dis 2014; 38: 633–46.
Tarcha EJ, Chi V, Munoz-Elias EJ, Bailey D, Londono LM, Upadhyay SK, et al. Durable pharmacological responses from the peptide ShK-186, a specific Kv1.3 channel inhibitor that suppresses T cell mediators of autoimmune disease. J Pharmacol Exp Ther 2012; 342: 642–53.
Tarcha EJ, Olsen CM, Probst P, Peckham D, Muñoz-Elías EJ, Kruger JG, Iadonato SP. Safety and pharmacodynamics of dalazatide, a Kv1.3 channel inhibitor, in the treatment of plaque psoriasis: a randomized phase 1b trial. PLoS One 2017; 12: e0180762.
Town T, Tan J, Flavell RA, Mullan M. T-cells in Alzheimer's disease. Neuromolecular Med 2005; 7: 255–64.
Villeda SA, Plambeck KE, Middeldorp J, Castellano JM, Mosher KI, Luo J, et al. Young blood reverses age-related impairments in cognitive function and synaptic plasticity in mice. Nat Med 2014; 20: 659–63.
Wang HR, Wu M, Yu HB, Long SY, Stevens A, Engers DW, et al. Selective inhibition of the k(ir)2 family of inward rectifier potassium channels by a small molecule probe: the discovery, SAR, and pharmacological characterization of ML133. ACS Chem Biol 2011; 6: 845–56.
Wang Q, Rowan MJ, Anwyl R. Beta-amyloid-mediated inhibition of NMDA receptor-dependent long-term potentiation induction involves activation of microglia and stimulation of inducible nitric oxide synthase and superoxide. J Neurosci 2004; 24: 6049–56.
Wulff H, Calabresi PA, Allie R, Yun S, Pennington M, Beeton C, et al. The voltage-gated Kv1.3 K(+) channel in effector memory T cells as new target for MS. J Clin Invest 2003; 111: 1703–13.
Wulff H, Castle NA, Pardo LA. Voltage-gated potassium channels as therapeutic targets. Nat Rev Drug Discov 2009; 8: 982–1001.

Wulff H, Knaus HG, Pennington M, Chandy KG. K+ channel expression during B cell differentiation: implications for immunomodulation and autoimmunity. J Immunol 2004; 173: 776–86.

Wulff H, Kolski-Andreaco A, Sankaranarayanan A, Sabatier JM, Shakkottai V. Modulators of small- and intermediate-conductance calcium-activated potassium channels and their therapeutic indications. Curr Med Chem 2007; 14: 1437–57.

Xiao C, Davis FJ, Chauhan BC, Viola KL, Lacor PN, Velasco PT, et al. Brain transit and ameliorative effects of intranasally delivered anti-amyloid-beta oligomer antibody in 5XFAD mice. J Alzheimers Dis 2013; 35: 777–88.

Zaritsky JJ, Redell JB, Tempel BL, Schwarz TL. The consequences of disrupting cardiac inwardly rectifying K+ current (I-K1) as revealed by the targeted deletion of the murine Kir2.1 and Kir2.2 genes. J Physiol-London 2001; 533: 697–710.

Zhang B, Gaiteri C, Bodea LG, Wang Z, McElwee J, Podtelezhnikov AA, et al. Integrated systems approach identifies genetic nodes and networks in late-onset Alzheimer's disease. Cell 2013; 153: 707–20.